CrystEngComm

ROYAL SOCIETY OF CHEMISTRY

PAPER

View Article Online
View Journal | View Issue

Cite this: *CrystEngComm*, 2024, **26**, 2784

Te···I secondary-bonding interactions in crystals containing tellurium(II), tellurium(IV) and iodide atoms: supramolecular aggregation patterns, nature of the non-covalent interactions and energy considerations†

Rosa M. Gomila, Antonio Frontera * and Edward R. T. Tiekink *

This study delves into the intriguing realm of chalcogen-bonding interactions, specifically focusing on tellurium(II) and/or tellurium(IV) interactions with iodide species within six crystals. Utilising comprehensive computational chemistry calculations and underpinned by crystallographic data retrieved from the Cambridge Structural Database, this research elucidates the supramolecular aggregation, bonding nature and interaction energetics of Te···I non-covalent bonds in a series of crystals containing each of tellurium(II), tellurium(IV) and iodide. The investigation encompasses a variety of molecular assemblies, ranging from zero-dimensional to complex three-dimensional architectures. Tellurium(II) atoms formed Te···I interactions in six of the crystals but tellurium(IV) participated in Te···I interactions in only three crystals despite there being equal numbers of tellurium(II) and tellurium(IV) atoms in the zero- and one-dimensional assemblies. Several computational tools, including Molecular Electrostatic Potential (MEP) surfaces, Quantum Theory of Atoms in Molecules (QTAIM) and Natural Bond Orbital (NBO) analyses, provide a nuanced understanding of the electron density topology and charge transfer mechanisms. In some assemblies, where the Te···I interactions are ~3.2 Å, the interaction energies are very large, *i.e.* 25.6 to 38.8 kcal mol^{-1}, suggesting partial covalent character, an observation corroborated by the NBO analysis; longer Te···I separations correlate with reduced energies, *i.e.* 3.1 to 7.0 kcal mol^{-1}. Crucially, it is noteworthy that the Te···I interactions identified in this study are distinctly characterised as chalcogen bonds, rather than halogen bonds.

Received 27th March 2024,
Accepted 3rd May 2024

DOI: 10.1039/d4ce00305e

rsc.li/crystengcomm

1. Introduction

In molecular crystals, tellurium has long been known to expand its coordination sphere to accommodate proximate atoms at separations longer than the sum of the covalent radii but shorter than the sum of the van der Waals radii; usually these intermolecular contacts introduce distortions in the central atom's coordination geometry.[1–9] The term "secondary-bonding" emerged as the all-encompassing description of these types of interactions operating in crystals of the main group elements.[10–12] While the atoms forming intermolecular interactions with tellurium are usually the lighter chalcogens, *i.e.* oxygen and sulphur, and halides, more recently, tellurium(lone-pair)···π(aryl) interactions have been recognised as important in providing stabilising interactions in crystals where such interactions can form.[13–15] There are three readily accessed oxidation states for tellurium, namely +II, +IV and +VI, having two, one and zero stereochemically active lone-pair of electrons, respectively. The interaction of electron-rich tellurium(II)/(IV) species with electron-rich donors, such as sulphur and iodide, is often rationalised in terms of the σ-hole concept.[16–19] This explanation for the interaction between these electron-rich species relates to an electron-deficient region at the extension of a covalent bond capable of interacting with nucleophiles such as lone-pairs of electrons and π-systems. The electrophile is normally attached to an electron-withdrawing group and increasing polarizability of the bond correlates with a greater σ-hole – thus, of the group 16 elements, the σ-hole will be at a maximum for tellurium.

When the electrophile is a chalcogen atom, the σ-hole model is given the specific term chalcogen-bonding[20] with these non-covalent connections capable of providing structure-directing interactions in crystals.[21] However,

Department of Chemistry, Universitat de les Illes Balears, Crta de Valldemossa km 7.5, 07122 Palma de Mallorca, Spain. E-mail: toni.frontera@uib.es, edward.tiekink@uib.es

† Electronic supplementary information (ESI) available: Images of additional supramolecular association for **1**–**5**. See DOI: https://doi.org/10.1039/d4ce00305e

systematic reviews of crystals featuring Se···O,[22] Se···N,[23,24] Se···π(aryl),[25] Te···N,[9] Te···I (ref. 26) and Te···π(aryl)[14] interactions confirm these contacts do not always arise from the interaction of a chalcogen-bound σ-hole with a nucleophile. Indeed, the situation is rather more complicated, especially in systems where an interacting atom forms multiple secondary-bonding interactions. Other interactions are sometimes observed, such as π-hole interactions, where the electron deficient region is located perpendicular to a framework sustained by covalent bonds.[27–29] In crystals of chalcogen-containing molecules, π-hole interactions can cooperate with σ-hole interactions[30–32] or even operate independently.[33,34] Instances of bifurcated[35–37] and charge-assisted[38,39] chalcogen bonds are also known. Computational chemistry calculations on the aforementioned neutral systems[31–37] and other non-charged systems[26,40] confirm that the energy imparted by the different interactions involving the tellurium are like or exceed those imparted by conventional hydrogen bonding.[41]

While the focus of the present study is upon the crystals, secondary-bonding interactions are known to persist in solution,[42,43] with recent studies highlighting the presence of intramolecular Te···F (ref. 44) contacts in solution, and the gas-phase (Te···N).[45] With such persistence, it is not surprising that chalcogen-bonding finds applications[46] beyond the solid-state[47] such as in coordination chemistry,[48] catalysis,[49,50] molecular recognition[51] and materials science.[52] While less numerous, chalcogen-bonding has many parallels with the ubiquitous halogen-bonding.[53]

The importance of strong and directional halogen-bonding in many spheres of endeavour[54] have been summarised in many reviews focussing upon catalysis,[55–57] liquid crystals,[58] polymer science,[59] phosphorescent materials,[60] molecular recognition,[61] *etc.* in addition to crystal engineering considerations.[62–64]

Of the halogens, the largest, iodide, is expected have the greatest σ-hole.[16] This was demonstrated in a bibliographic review of X···π(aryl), for X = I, Br, Cl and F, interactions in crystals.[65] Thus, delocalised[66] I···π(aryl) interactions in crystals did not necessarily persist in crystals of the lighter congeners. However, other factors must come into play as demonstrated in a survey of competing I···Br interactions,[67] which saw a 1 : 2 ratio of type I to type II[68,69] I···Br interactions, showing the σ-hole on iodide is not all pervasive and subject to other considerations in crystals. In the present work, a survey and computational chemistry investigation of Te···I interactions formed in heterovalent[70,71] crystals containing both tellurium(II) and tellurium(IV) as well as iodide is described. The aim of the work is to determine the propensity of formation, competition, *i.e.* $Te^{II}\cdots I$ *vs.* $Te^{IV}\cdots I$, nature and energies of stabilisation provided by the identified Te···I interactions.

2. Methods

The data in the Cambridge Structural Database (CSD; version 5.44, April 2023)[72] was searched using ConQuest (version 2023.1.0).[73] The analysis sought all crystal structures having an intermolecular Te···I interaction less than or equal to the sum of the van der Waals radii of tellurium (2.06 Å) and iodide (1.98 Å), *i.e.* 4.04 Å,[74] in crystals containing tellurium and iodide. Additional criteria were applied in that only molecular single-crystal structures with three-dimensional coordinates and $R \leq 0.075$ were sought and having no errors nor disorder and were charge neutral. Manual inspection of the 269 "hits" retrieved nine mixed tellurium(II)/tellurium(IV) structures and six of these had Te···I interactions between non-charged species and operating independently of alternate, directional intermolecular interactions. The analysis of the six crystals was conducted with PLATON[75] and DIAMOND.[76] All crystallographic diagrams in section 3.1 and ESI† Fig. S1–S5 are original, being generated using DIAMOND.[76]

The computational chemistry calculations were carried out with the Turbomole 7.7 program,[77] using the crystallographic coordinates available in the respective CIFs as input for the evaluation of the supramolecular assemblies. The positions of the hydrogen atoms were optimised in dimers where hydrogen bonds are established. The level of theory used for the calculations was PBE0 (ref. 78)-D4 (ref. 79)/def2-TZVP.[80,81] For heavier elements, such as tellurium and iodide, this basis set includes effective core potentials (ECPs) and takes into consideration relativistic effects for the inner electrons.[81] This combination of method and basis set has been previously used by us[82] and others[83] to analyse σ-hole interactions, including chalcogen bonds (ChBs) involving tellurium.[26] The MEP surface plots were generated using the wavefunction obtained at the same level of theory and 0.001 a.u. isosurfaces. The topological analysis of the electron density was carried out according to the quantum theory of atoms in molecules (QTAIM) method proposed by Bader[84] and represented using the VMD program.[85] The NBO analysis[86] was performed using the same level of theory and the NBO7.0 program.[87] The NBOs and charge density plots were represented using the VMD software.[85]

3. Results and discussion

The chemical diagrams for the six systems investigated herein by a range of theoretical procedures are presented in Fig. 1. Based on the standard van der Waals radii assumed in PLATON,[75] two, three and one zero-, one- and three-dimensional aggregation patterns, respectively, featuring Te···I interactions functioning independently of alternative non-covalent interactions, such as conventional hydrogen-bonding and I···I halogen-bonding, have been identified.

3.1 Supramolecular aggregation

Table 1 presents a summary of the coordination number (CN) and donor sets for the tellurium atoms participating in Te···I interactions as well as salient geometric parameters characterising these.

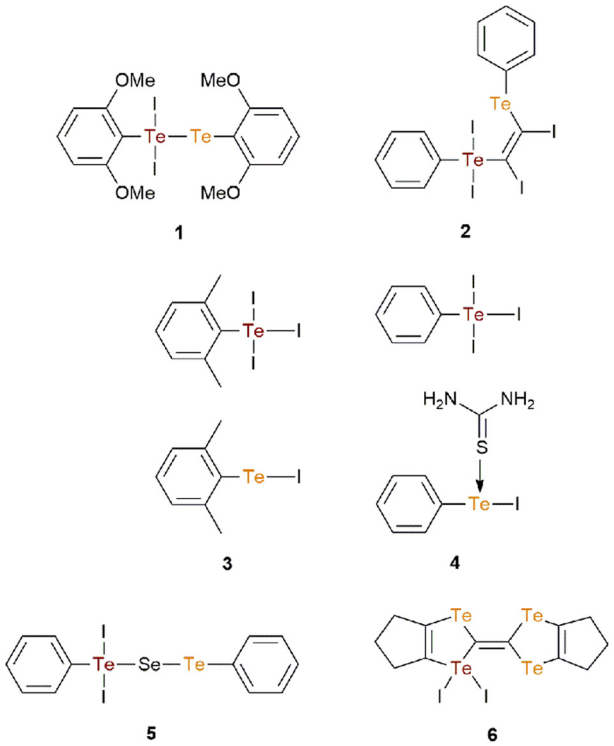

Fig. 1 Chemical diagrams for the mixed tellurium(II)/tellurium(IV) iodide species investigated herein, **1**–**6**. Compounds **3** and **4** are 1:1 co-crystals with the coformers being connected by Te···I interactions in their respective crystals.

The first and simplest aggregate to be described is formed in the crystal of ditellane, $L^1Te^{II}Te^{IV}I_2L^1$ for L^1 = 2,6-dimethoxyphenyl (**1**).[88] Here, the tellurium(II) atom forms a Te···I interaction with one of the tellurium(IV)-bound iodide atoms over a centre of inversion to form a dimer. As shown in ESI† Fig. S1(a), the aggregation results in the formation of a flat, six-membered $\{\cdots Te_2I\}_2$ synthon. Within the aggregate, intramolecular Te···O interactions are noted, with the shortest Te···O separation being 2.905(4) Å. In the crystal, the dimeric aggregates assemble into a chain *via* relatively long I···I halogen-bonding interactions; see ESI† Fig. S1(b). A very similar mode of aggregation as for **1**, is found in the crystal of $PhTe^{II}C(I)=C(I)Te^{IV}PhI_2$ (**2**),[89] but results in a twisted, centrosymmetric 10-membered synthon $\{\cdots TeC_2TeI\}_2$, ESI† Fig. S2(a). An intramolecular $Te^{II}\cdots Te^{IV}$ interaction [3.4205(4) Å] is noted. The aggregates are connected into a three-dimensional architecture *via* I···I halogen-bonding; see ESI† Fig. S2(b) for details.

There are three examples of one-dimensional aggregation patterns. The first of these, formulated as (2,6-dimethyphenyl)$ITe^{II}(\mu$-I)Te^{IV}(2,6-dimethyphenyl)I_2,[90] **3**, resembles those of **1** and **2** in that it is only the tellurium(II) atom that forms Te···I interactions within the aggregation pattern with the notable difference being that the tellurium(II) atom engages in two Te···I interactions, Fig. 2(a), with one separation being, (i), being significantly shorter than the second, (ii). The tellurium(II) atom is tri-coordinated within a CI_2 donor set as one of the tellurium(IV)-bound iodide atoms links the two tellurium atoms; the bridge is close to symmetric with the Te^{IV}–I bond length [2.9130(3) Å] being marginally shorter than the Te^{II}–I bond [3.0267(3) Å]; the tellurium(IV) atom is coordinated within a C_3I donor set. The molecules assemble through centrosymmetric, four-membered $\{\cdots Te\cdots I\}_2$ synthons which are flat and are linked *via* larger, eight-membered $\{\cdots TeITeI\}_2$ synthons. These latter synthons are also centrosymmetric and have the form of an elongated chair with the iodide atoms engaged in the Te···I interactions lying above and below the plane defined by the remaining atoms. Only one of the iodide atoms participates in the formation of Te···I interactions. The Te···I interactions feature within a supramolecular ribbon, Fig. 2(a). The presence of I···I halogen-bonding in the crystal of **3** lead to the formation of two-dimensional arrays; see ESI† Fig. S3(b).

The molecule in the 1:1 co-crystal **4** has the formula $PhTe^{II}I[S=C(NH_2)_2]\cdot PhTe^{IV}I_3$.[91] The tellurium(II) centre is tri-coordinated by the *ipso*-carbon atom of a phenyl group, an iodide and a loosely bound thione-sulphur atom of a thiourea molecule, while the tellurium(IV) atom is tetra-coordinated by the *ipso*-carbon atom of a phenyl group and three iodide atoms. Each of the independent tellurium(II) and tellurium(IV) atom participates in the formation of Te···I interactions

Table 1 Listing of coordination numbers (CN), donor sets, Te···I separations and selected angles for **1**–**5**

Aggregate/interaction[a]	Te^{II} – CN/donor set	Te^{IV} – CN/donor set	*d*(Te···I) (Å)	Y–Te···I (°)
1/(i)/Te^{II}	2/$Te^{IV}C$	4/$Te^{II}I_2C$	4.0169(5)	Y = Te^{IV}, 157.377(15)
2/(i)/Te^{II}	2/C_2	4/I_2C_2	3.7708(4)	Y = ethylene-C, 171.97(11)
3/(i)/Te^{II}	2/CI_2	4/CI_3	3.2175(4)	Y = I, 173.288(11)
3/(ii)/Te^{II}	3/CI_2	4/C_3I	3.9902(4)	Y = Te^{IV}, 153.679(10)
4/(i)/Te^{IV}	3/CIS	4/CI_3	3.2651(7)	Y = I, 174.501(19)
4/(ii)/Te^{IV}			3.7601(14)	Y = phenyl-C, 174.08(16)
4/(iii)/Te^{II}			3.5063(8)	Y = Te^{IV}, 170.20(2)
4/(iv)/Te^{II}			3.9034(14)	Y = phenyl-C, 157.14(16)
5/(i)/Te^{IV}	2/CSe	4/CI_2Se	3.9424(10)	Y = Se, 171.40(3)
5/(ii)/Te^{IV}			3.9712(10)	Y = phenyl-C, 170.3(2)
5/(iii)/Te^{II}			3.9925(10)	Y = phenyl-C, 166.4(2)
5[b]/(iv)/Te^{II}			3.8910(10)	Y = Te^{IV}, 73.40(2); Y = Se, 93.36(3); Y = phenyl-C, 92.9(2)

[a] The interaction is as in Fig. 2. [b] This interaction is intramolecular.

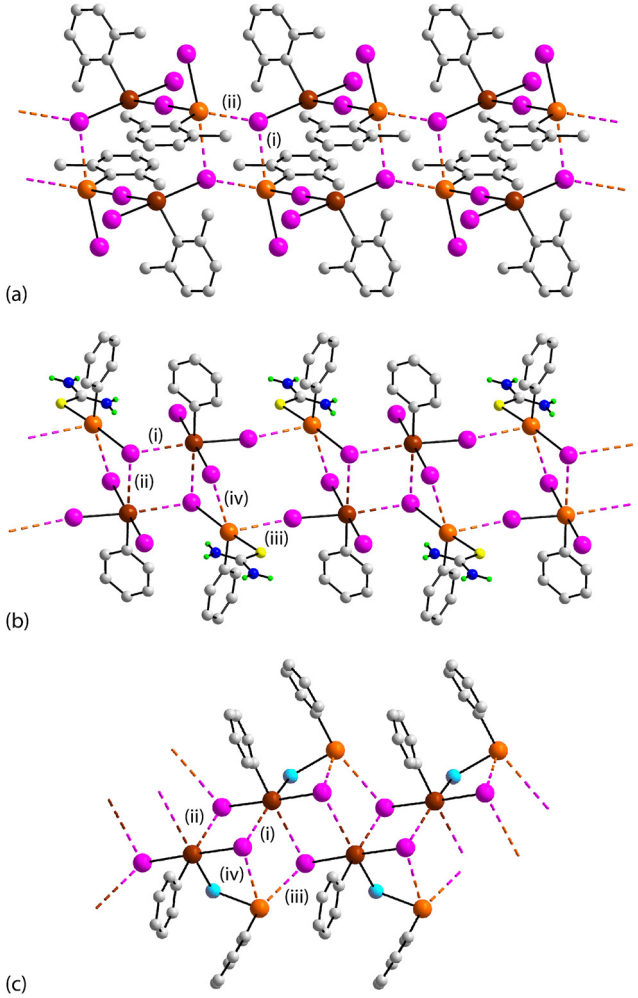

Fig. 2 Views of the supramolecular ribbons featuring Te···I interactions in the crystals of (a) **3**, (b) **4** and (c) **5**.

leading to three distinct synthons. The tellurium(II)-bound iodide forms two Te···I interactions while two of the tellurium(IV)-bound iodide atoms form Te···I interactions. Referring to Fig. 2(b), centrosymmetric, four-membered $\{\cdots Te^{IV}\cdots I\}_2$ synthons, resembling those seen in **3**, involve tellurium(IV) atoms exclusively. Here, each of the tellurium(IV) and tellurium(II)-bound iodide atoms forms two Te···I interactions. Larger, centrosymmetric and eight-membered $\{\cdots Te^{II}\cdots ITe^{IV}I\}_2$ synthons are constructed from the tellurium(II) atom forming two Te···I interactions with two independent tellurium(IV)-bound iodide atoms. The third synthon, is non-symmetric and four-membered $\{\cdots Te^{II}$-$I\cdots Te^{IV}I\}$. This is the first synthon to be described herein involving tellurium in both the +II and +IV oxidation states. The Te···I separations in this latter synthon are the longest of the four independent Te···I interactions. In the crystal, I···I halogen-bonding combine with N–H···I hydrogen-bonds to form a double-layer; see ESI† Fig. S4.

The third one-dimensional aggregation is seen in the crystal of **5** which comprises binuclear molecules formulated as $PhTe^{II}(\mu\text{-}Se)Te^{IV}PhI_2$.[92] In terms of Te···I interactions, each independent tellurium atom forms two such interactions as does each of the two independent, tellurium(IV)-bound iodide atoms; all separations are long, Table 1. A non-symmetric, four-membered $\{\cdots Te^{IV}I\}_2$ synthon is formed where tellurium(IV) atoms arranged in a zigzag fashion along the glide plane are bridged by the two independent iodide atoms. The synthons are corner-shared through the tellurium(IV) atoms to form a ribbon and represented by entries (i) and (ii) in Fig. 2(c). A second, non-symmetric and four-membered $\{\cdots Te^{II}I\cdots Te^{IV}I\}$ synthon, like that seen in the crystal of **4**, provides additional links between the $\{\cdots Te^{IV}I\}_2$ synthons, *i.e.* entries (iii) and (iv); these additional Te···I interactions involve the tellurium(II) atom. The overall assembly features concatenated and alternating four-membered synthons. The ribbons are connected into a two-dimensional array *via* centrosymmetric $\{\cdots Te^{II}Se\}_2$ synthons as illustrated in ESI† Fig. S5.

There is a sole example where molecules are assembled within a three-dimensional architecture with Te···I interactions between the molecules operating in three dimensions. The tetra-tellurium molecule, **6**, hexamethylenetetratellurafulvalene di-iodide,[93] comprises a single tellurium(IV) site with three positions occupied by tellurium(II) atoms in the inner five-membered rings, Fig. 1. Owing to its complexity, computational chemistry was not conducted on this crystal so the description of the molecular packing along with diagrams is included in ESI† Fig. S6.

3.2 Theoretical study

A detailed theoretical investigation of the specific assemblies inclusive of Te···I interactions in **1**–**5** has been conducted with a focus upon an exploration of the nature of the non-covalent bonding interactions through various computational techniques. As highlighted in section 3.1, these interactions play a crucial role in determining the dimensionality of the assemblies and crystal structure organisation. The analysis commences with the zero-dimensional aggregates identified in the crystals of **1** and **2**.

The molecular electrostatic potential (MEP) surface for the molecule in dimeric **1**, depicted in Fig. 3(a), reveals that the MEP maximum is positioned at the hydrogen atoms of the methoxy groups, registering at +26.3 kcal mol^{-1}. The anticipated σ-holes on the tellurium(IV) and tellurium(II) atoms are mostly masked by the intramolecular interactions with the lone-pairs (LPs) on the oxygen atoms of the methoxy groups, which are orientated towards the tellurium atoms. Notably, a σ-hole on the tellurium(II) atom remains partially accessible, attributed to the rotation of the dimethoxyphenyl ring, and measures +7.5 kcal mol^{-1}. The MEP minimum, indicating nucleophilic regions, is found at the iodide atom, *i.e.* −32.7 kcal mol^{-1}. The larger MEP value at the hydrogen atoms compared to the tellurium atoms suggests that this molecule is more predisposed to forming hydrogen bonds, *e.g.* CH···I, rather than chalcogen bonds.

The Quantum Theory of Atoms in Molecules (QTAIM) analysis of the self-assembled dimer, illustrated in Fig. 3(b),

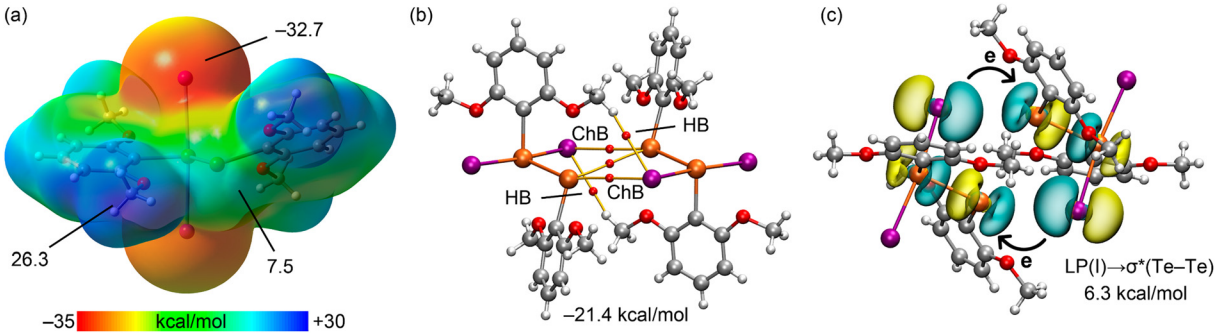

Fig. 3 (a) MEP surface of the molecule in **1** with isosurface 0.001 a.u., (b) QTAIM analysis (BCPs are represented as red spheres and bond paths as orange lines; only intermolecular contacts are indicated for clarity) and (c) plot of the NBOs involved in the chalcogen bonds (ChB). Stabilisation energies are indicated in (b) and (c). HB = hydrogen bond.

validates the presence of Te···I interactions through bond critical points (BCPs) and bond paths linking the tellurium and iodide atoms. Additionally, this analysis identifies two symmetric CH···I contacts, corroborating the MEP findings. The QTAIM analysis also reveals the existence of a BCP and a bond path interconnecting the tellurium(II) atoms suggesting a van der Waals interaction between them. The dimerization energy is significantly great at −21.4 kcal mol^{-1}, due to the cooperation of both interactions. The density (ρ), the Lagrangian kinetic energy density (G), the potential energy density (V) the total energy density (H) and the Laplacian ($\nabla^2\rho$) of the electron density values at the BCPs represented in Fig. 3(b) are collated in Table 2. The positive values of H and $\nabla^2\rho$ along with low values of ρ, confirm the non-covalent nature of the interactions. Higher values of ρ and V at the BCPs associated with chalcogen bonds indicate that these are the predominant forces driving the formation of the dimer.

Table 2 QTAIM parameters in a.u. measured at the bond critical points shown in Fig. 3–7. The atom labels correspond to those of the X-ray structures (retrieved from the respective CIFs). See also Fig. 2 for the labelling of some interactions

	ρ	$G(r)$	$V(r)$	$H(r)$	$\nabla^2\rho$
1					
Te1–Te2	0.0071	0.0028	−0.0025	0.0004	0.0128
Te2···I1 (i)	0.0073	0.0033	−0.0027	0.0006	0.0155
C13-H7···I1	0.0037	0.0020	−0.0015	0.0005	0.0099
2					
Te2···I2 (i)	0.0108	0.0050	−0.0045	0.0005	0.0219
Te2···Te2	0.0049	0.0019	−0.0016	0.0003	0.0090
Te1···C10	0.0098	0.0056	−0.0048	0.0008	0.0257
3					
C2–H3···I1	0.0052	0.0030	−0.0023	0.0007	0.0147
Te2···I2 (i)	0.0301	0.0117	−0.0149	−0.0032	0.0341
Te1···C7	0.0094	0.0053	−0.0045	0.0008	0.0247
C9–H8···I2	0.0072	0.0041	−0.0034	0.0008	0.0198
C15–H15···C5	0.0069	0.0044	−0.0035	0.0009	0.0210
4					
Te2···I1 (iv)	0.0096	0.0044	−0.0039	0.0005	0.0193
Te2···I3 (ii)	0.0119	0.0054	−0.0051	0.0004	0.0232
Te2···I2	0.0060	0.0025	−0.0021	0.0004	0.0117
C4–H3···C12	0.0043	0.0028	−0.0021	0.0008	0.0145
C6–H5···C9	0.0050	0.0032	−0.0024	0.0008	0.0159
Te1···I3 (i)	0.0293	0.0108	−0.0136	−0.0028	0.0322
5					
Te1···I2 (i)	0.0093	0.0038	−0.0034	0.0004	0.0170
C4–H3···I2	0.0056	0.0031	−0.0024	0.0007	0.0150
Te2···I2 (iii)	0.0075	0.0035	−0.0029	0.0006	0.0167
Te2···C8	0.0100	0.0054	−0.0047	0.0008	0.0248
Te1···I1 (ii)	0.0080	0.0037	−0.0031	0.0005	0.0168

Charge transfer effects were examined next using Natural Bond Orbital (NBO) analysis, with the relevant NBOs involved in the chalcogen bonds show cased in Fig. 3(c). This analysis illustrates electron donation from the LP at the iodide atom to the anti-bonding orbital, σ*(Te^{II}–Te^{IV}), resulting in a total stabilisation energy of 6.3 kcal mol^{-1} for the two LP(I) → σ*(Te^{II}–Te^{IV}) contributions. This relatively modest orbital contribution is consistent with the elongated Te···I experimental distance of 4.0169(5) Å.

A similar analysis was conducted for dimeric **2**, where the MEP surface distinctly illustrates the σ-holes on both tellurium(II) and tellurium(IV) atoms, Fig. 4(a), exhibiting comparable energies of +24.8 and +24.3 kcal mol^{-1}, respectively. The MEP minimum is found at the iodide atom's negative belt, marked by −16.9 kcal mol^{-1}. Moreover, the MEP highlights negative potential, *i.e.* −8.8 kcal mol^{-1}, over the π-system of the aromatic ring, suggesting regions prone to electron donation.

The QTAIM analysis, as shown in Fig. 4(b), confirms the engagement of both σ-holes in chalcogen-bonding interactions. Each Te^{II}···I interaction is delineated by a BCP and a bond path that connects the tellurium and iodide atoms. Intriguingly, the QTAIM analysis further reveals a BCP and bond path linking the tellurium(IV) atom to a carbon atom within the aromatic ring, demonstrating the formation of two additional chalcogen bonds within the aggregate with the π-systems serving as electron donors as highlighted in the inset plot of Fig. 4(b). A BCP and bond path linking the two tellurium(II) atoms were also observed, indicating an interaction between these atoms. The QTAIM data at the BCPs (Table 2) is typical of non-covalent interactions, with positive values of H and $\nabla^2\rho$.

The interaction energy for the aggregate in **2** is significantly negative (−28.2 kcal mol^{-1}) and is predominantly attributed to the chalcogen bonds, as corroborated by the QTAIM data of Table 2. Moreover, the QTAIM values are

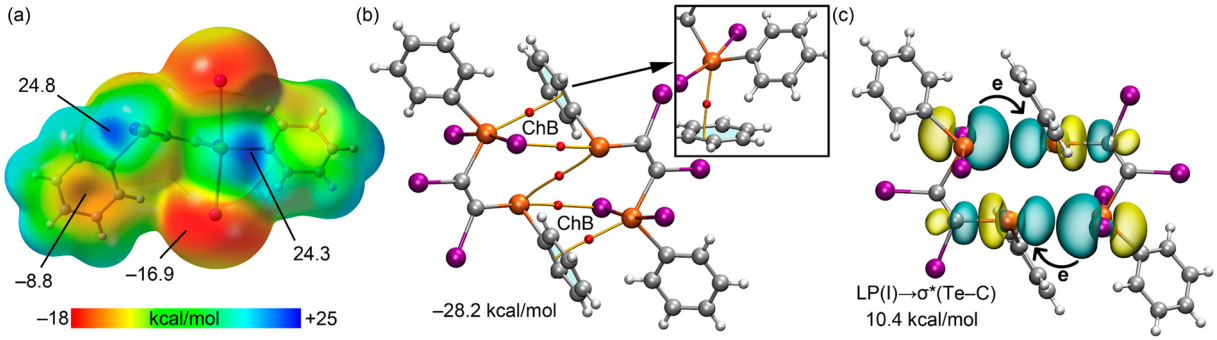

Fig. 4 (a) MEP surface of molecule **2** with isosurface 0.001 a.u., (b) QTAIM analysis (BCPs are represented as red spheres and bond paths as orange lines; only intermolecular contacts are indicated for clarity) and (c) plot of the NBOs involved in the chalcogen bonds (ChB). Stabilisation energies are indicated in (b) and (c).

larger in **2** with respect to **1** at the Te···I BCPs, consistent with the larger binding energy of the former. The NBO analysis elucidates the lone-pairs (LPs) at the iodide atoms are precisely aligned with the anti-bonding σ*(Te^{II}–C) orbitals, Fig. 4(c). This alignment results in a total stabilisation energy (10.4 kcal mol^{-1}) surpassing that observed for the aggregate in **1**. This greater stabilisation energy in **2** correlates with the shorter Te···I distance of 3.7708(4) Å (*cf.* 4.0169(5) Å in **1**) and enhanced directionality (the I···Te–C angle is 171.97(11)° *cf.* I···Te^{II}–Te^{IV} = 157.377(15)° in **1**), indicating a stronger and more directed chalcogen-bonding interaction in **2** compared to **1**.

Beyond the zero-dimensional assemblies of **1** and **2**, the analysis extends to the chalcogen bonds in the crystal featuring supramolecular tapes, starting with **3**, with a particular focus on the shorter Te···I interaction (labelled as (i) in Fig. 2(a), and distance = 3.2175(4) Å). The longest chalcogen bond interaction (3.9902(4) Å, labelled as (ii) in Fig. 2(a)), is not discussed in detail because it is similar to those already analysed in **1** and **2**. The MEP surface of the molecule in **3**, Fig. 5(a), reveals a pronounced σ-hole on the tellurium(II) atom opposite the Te^{II}–I bond, showing a high potential of +40.8 kcal mol^{-1}, and a less intense σ-hole opposite the Te^{II}–C bond, with a potential of +21.3 kcal mol^{-1}. Additionally, the MEP is positive around the hydrogen atom of the methyl groups (+19.5 kcal mol^{-1}), with the MEP minimum once again located at one of the iodide atoms (−31.4 kcal mol^{-1}), echoing the findings for **1**. The significant MEP values at both the iodide and tellurium atoms suggest the likelihood of strong chalcogen-bonding interactions.

The QTAIM analysis of the dimer reveals a complex arrangement of BCPs and bond paths, Fig. 5(b). Besides the BCPs and bond paths indicative of chalcogen bonds, the presence of methyl groups promotes the formation of additional CH···I and CH···π interactions, characterised by BCPs and bond paths connecting the hydrogen atoms to iodide and aromatic-C atoms, respectively. This complex network of interactions contributes to a notably strong dimerization energy, *i.e.* −59.5 kcal mol^{-1}. The QTAIM parameters in Table 2 for **3** corroborate the chalcogen bonds are the strongest interactions. Moreover, one chalcogen bond presents a negative value of H, suggesting a partial covalent interaction. Furthermore, the NBO analysis presented in Fig. 5(c) reveals charge transfer from the iodide-bound lone-pair (LP) to the anti-bonding σ*(Te^{II}–I) orbital is exceptionally substantial (51.2 kcal mol^{-1} in total), nearly mirroring the total interaction energy. This finding strongly implies partial covalent nature for these chalcogen bonds in line with the QTAIM analysis and underscores the significant role of electron donation in stabilising these interactions.

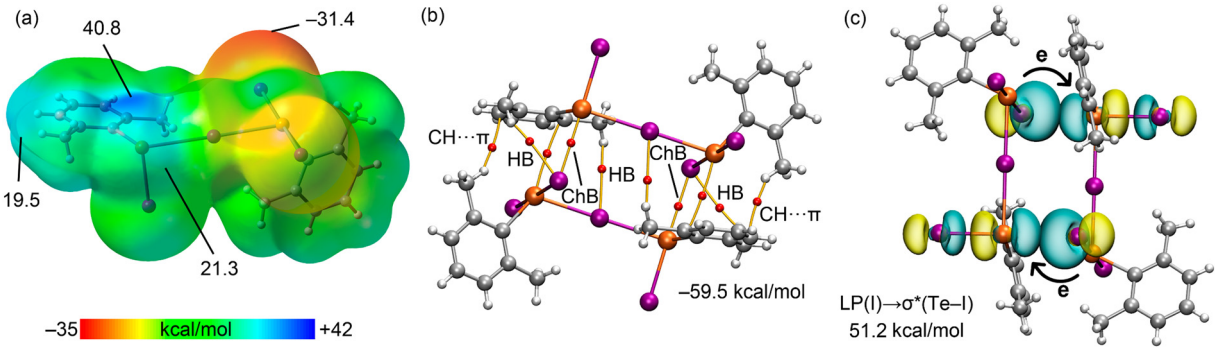

Fig. 5 (a) MEP surface of **3** with isosurface 0.001 a.u., (b) QTAIM analysis (BCPs are represented as red spheres and bond paths as orange lines; only intermolecular contacts are indicated for clarity) and (c) plot of the NBOs involved in the chalcogen bonds. Stabilisation energies are indicated in (b) and (c).

The chalcogen bonds within the 1 : 1 co-crystal **4** have also been analysed theoretically with an emphasis on the distinct interactions involving the tellurium(IV) centre as the $Te^{II}\cdots I$ interactions resemble those already analysed in detail in **3**. The MEP surfaces for both coformers are illustrated in Fig. 6(a). For the tellurium(IV)-containing coformer, the MEP values at the σ-holes are 40.2 and 26.3 kcal mol^{-1}, and correspond to the regions at the extension of the Te–I and Te–C bonds, respectively; these values mirror the values seen in **3**. In the case of the second coformer, the attachment of thiourea to the tellurium(II) atom significantly diminishes the σ-hole opposite the Te^{II}–C bond, *i.e.* to 9.4 kcal mol^{-1}. As expected for this molecule, the MEP maximum is located at the thiourea-bound hydrogen atoms (90.0 kcal mol^{-1}). The MEP minima at the iodide atoms are −13.8 kcal mol^{-1} for $PhTe^{IV}I_3$ and −42.7 kcal mol^{-1} for $PhTe^{II}I[S{=}C(NH_2)_2]$, indicating a strong $Te^{IV}\cdots I$ interaction, supported by the short experimental distance of 3.2651(7) Å (interaction labelled as (i) in Fig. 2(b) *cf.* 3.7601(14) Å for interaction (ii) in Fig. 2(b)).

The distribution of BCPs and bond paths in the tetrameric assembly, shown in Fig. 6(b), verifies a complex network comprising up to eight Te···I interactions as well as CH···π contacts. As noted above, both tellurium(II) and tellurium(IV) function as σ-hole donors in establishing chalcogen bonds. The formation energy of this assembly is significantly great (−86.5 kcal mol^{-1}), again hinting at a partial covalent nature for the shorter chalcogen bonds. This covalent character is further confirmed by the NBO analysis, which examined both types of chalcogen bonds. For the $Te^{IV}\cdots I$ interactions, the stabilisation energy from the LP(I) → σ*(Te^{IV}–I) charge transfer is 77.5 kcal mol^{-1} (Fig. 6(c), left) underscoring the strong covalent character. This is further corroborated by the QTAIM parameters, Table 2, revealing a negative total energy density value (H = −0.0028 a.u.) and a significant charge density (0.0293 a.u.) compared to the remaining BCPs. Conversely, the stabilisation energy from the LP(I) → σ*(Te^{IV}–C) charge transfer (Fig. 6(c), right) is considerably lower (14.0 kcal mol^{-1}), consistent with the longer $Te^{IV}\cdots I$ distance, illustrating the varying strength and nature of these $Te^{IV}\cdots I$ interactions within the co-crystal.

In the final example to be analysed, the chalcogen bonds present in the crystal of **5** were evaluated. The MEP surface, depicted in Fig. 7(a), reveals two distinct σ-holes on each type of tellurium atom. Notably, the σ-holes opposite the Te–Se bonds on both tellurium(II) and tellurium(IV) atoms are equivalent, each valued at 25.0 kcal mol^{-1}, and those opposite the Te–C bonds are comparable, with values of 15.7 and 18.8 kcal mol^{-1} for the tellurium(II) and tellurium(IV) atoms, respectively. The MEP minimum is located on an

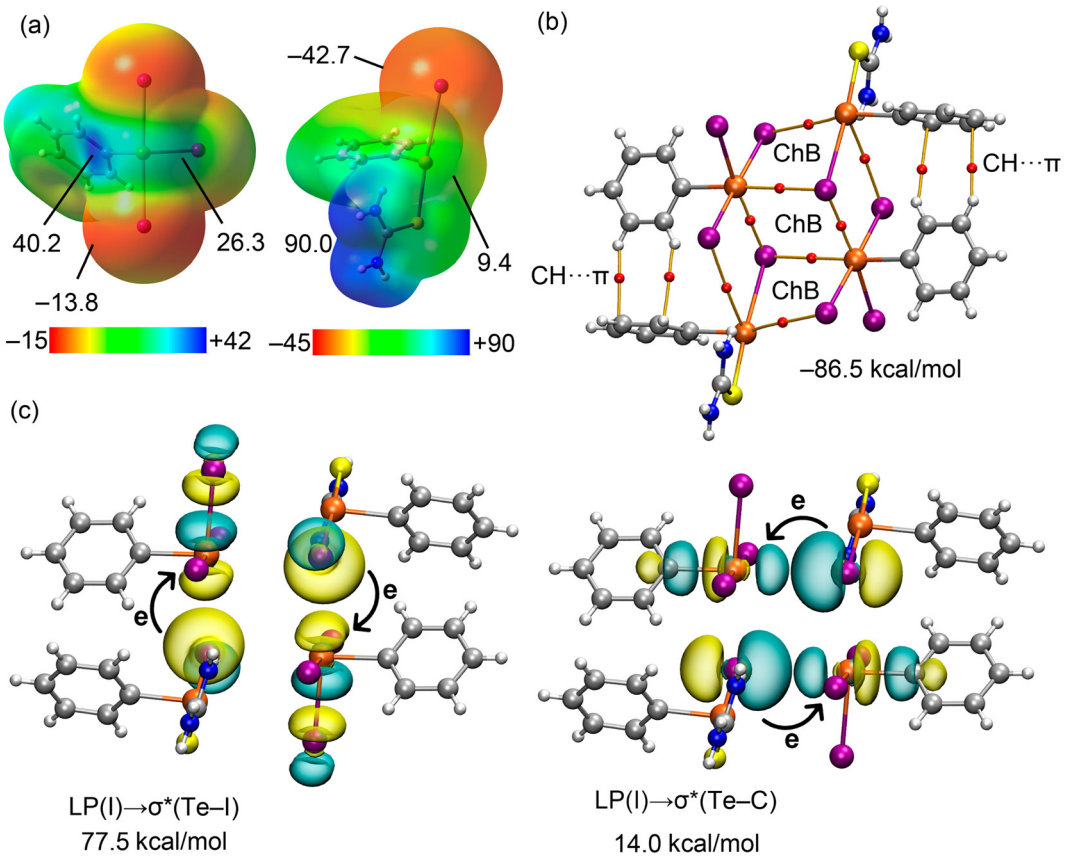

Fig. 6 (a) MEP surfaces of the two coformers of co-crystal **4** with isosurface 0.001 a.u., (b) QTAIM analysis (BCPs are represented as red spheres and bond paths as orange lines; only intermolecular contacts are indicated for clarity) and (c) plot of the NBOs involved in both types of chalcogen bonds. Stabilisation energies are indicated in (b) and (c).

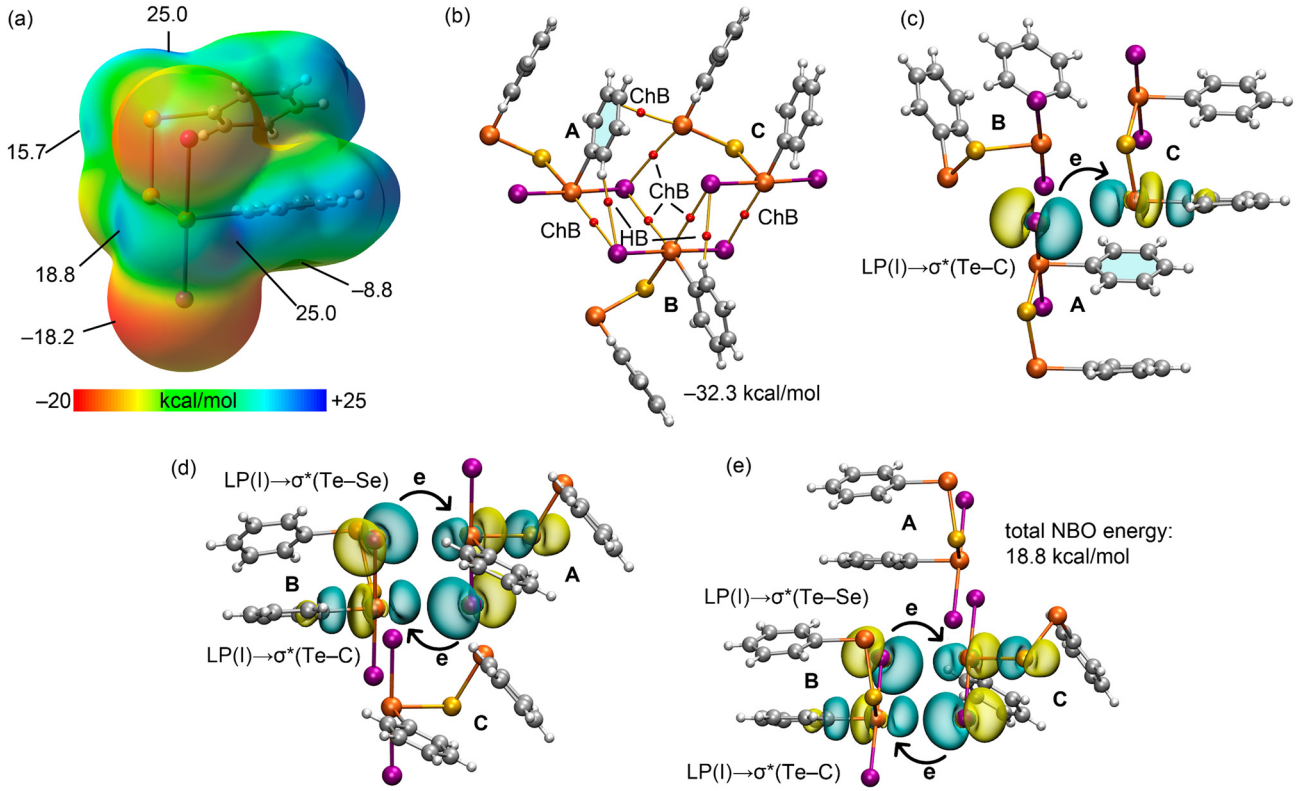

Fig. 7 (a) MEP surface of the molecule in **5** with isosurface 0.001 a.u., (b) QTAIM analysis (BCPs are represented as red spheres and bond paths as orange lines; only intermolecular contacts are indicated for clarity) and (c–e) plots of the NBOs involved in both types of chalcogen bonds. Stabilisation energies are indicated in (b) and (e).

iodide atom (−18.2 kcal mol^{-1}), with the MEP also showing nucleophilicity over the π-system of the aromatic ring.

A trimeric assembly of this compound, as presented in Fig. 7(b), was examined using the QTAIM method, which identifies five Te···I chalcogen bonds and one Te···π(aryl) interaction. In addition, the QTAIM analysis uncovers the presence of two CH···I hydrogen bonds. The trimerization energy, calculated at −32.3 kcal mol^{-1}, aligns well with the dimerization energies observed for the aggregates in **1** and **2**. All identified chalcogen bonds were further scrutinised using NBO analysis, which consistently observed lone-pair (LP) to anti-bonding σ* charge transfer across the interactions, *i.e.* LP(I) → σ*(Te–C) and LP(I) → σ*(Te–Se). Here, the cumulative stabilisation energy was 18.8 kcal mol^{-1}, suggesting the predominantly non-covalent character of these interactions. This aligns well with the QTAIM values (Table 2) with positive total energy density (H) values and ρ values that range from 0.0056 to 0.0100 a.u. An interesting point to note is the significance of all four σ-holes in the formation of the supramolecular tape illustrated in Fig. 2(c) and revealed by the QTAIM analysis, highlighting their critical role in the assembly of the molecules in the crystal.

4. Overview

Six crystals containing at least one each of tellurium(II), tellurium(IV) and iodide have been evaluated for their propensity to form Te···I interactions. In zero-dimensional **1** and **2**, and one-dimensional **3**–**5** there are equal numbers of tellurium(II) and tellurium(IV) atoms. In **1**–**3** the Te···I interactions involve tellurium(II) only, but in each of **4** and **5**, equal numbers of Te^{II}···I and Te^{IV}···I interactions are apparent; in three-dimensional **6**, there is a 3 : 1 ratio between tellurium(II) and tellurium(IV) atoms, and of the five Te···I interactions identified, four involve tellurium(II). The dominance of tellurium(II) over tellurium(IV) in forming Te···I interactions in this rather small data set may simply relate to steric crowding given the tellurium(II) atoms are usually two-coordinate whereas the tellurium(IV) centres are four-coordinate.

Prior to summarising the results of the computational chemistry investigations, it is salient to place the observed number of mixed tellurium(II), tellurium(IV) and iodide crystals featuring Te···I interactions in context. In the CSD[72] there are 207 independent, non-charged crystals containing both tellurium and iodide but excluding other metals. Following these criteria, there are seven examples of mixed tellurium(II), tellurium(IV) and iodide crystals, while each of these featured Te···I interactions one of the crystals saw these operating in concert with I···I interactions.[94] There are 71 examples of crystals containing tellurium(II) and iodide of which 15 (21%) contain Te···I interactions operating independently of other, structure-directing non-covalent interactions while there are 129 crystals containing

tellurium(IV) and iodide, 69 (54%) exhibit Te···I interactions operating independently of other obvious directional non-covalent interactions. These data suggest that tellurium(II) compounds are less likely to form Te···I interactions than tellurium(IV) compounds.

Comprehensive theoretical analyses, employing Molecular Electrostatic Potential (MEP), Quantum Theory of Atoms in Molecules (QTAIM) and Natural Bond Orbital (NBO) techniques, have elucidated the intricate chalcogen-bonding interactions across the series of compounds, **1**–**5**. These studies reveal the significant influence of σ-holes on the formation of chalcogen bonds and their subsequent impact on the structural dimensionality and stability of the observed molecular assemblies. From zero-dimensional aggregates to complex trimeric and tetrameric arrangements within one-dimensional tapes, the findings underscore the variability in interaction strengths, highlighting the covalent to non-covalent nature of these bonds. The discernible σ-holes, critical to the formation of supramolecular tapes, demonstrate the nuanced interplay between molecular geometry, electron density and interaction energy. It is also noteworthy to emphasise that the Te···I interactions identified in this study are characterized as chalcogen bonds rather than halogen bonds. This distinction is based on the directionality of the interactions and the observed positive and negative MEP values at the interacting atoms.

In terms of energies of stabilisation imparted by the identified Te···I interactions, these span a considerable range. Thus, while most of the interaction energies are generally small, *i.e.* ranging from 3.1 to 7.0 kcal mol^{-1} in **1**, **2** and **5**, these increase markedly in two examples, *i.e.* 25.6 to 38.8 kcal mol^{-1} in **3** and **4**, involving tellurium(II) and tellurium(IV) centres, respectively, where the Te···I separations are consistent with some covalent character.

5. Conclusions

When both tellurium(II) and tellurium(IV) atoms are present in iodide-containing crystals, a tellurium(II) atom will always form a Te···I interaction but not necessarily the tellurium(IV) atom. The Te···I interactions are always classified as chalcogen bonds being distinguished by the directionality of the interactions. This work not only advances the understanding of chalcogen bonds in supramolecular assembly/crystal engineering but also sets the groundwork for future exploration into the design and synthesis of novel materials guided by chalcogen-bonding principles.

Author contributions

Rosa M. Gomila: computational chemistry, investigation, visualisation, writing – original draft. Antonio Frontera: computational chemistry, investigation, visualisation, writing – original draft. Edward R. T. Tiekink: conceptualisation, CSD analysis, investigation, visualisation, writing – original draft.

Conflicts of interest

The authors declare no competing financial interest.

Acknowledgements

The authors thank the MICIU/AEI of Spain (project PID2020-115637GB-I00 FEDER funds) for financial support and the CTI (UIB) for computational facilities.

References

1 O. Foss, Stereochemistry of tellurium(II) complexes and related compounds, *Pure Appl. Chem.*, 1970, **24**, 31–48, DOI: **10.1351/pac197024010031**.
2 S. Husebye, Recent developments on the structural chemistry of complexes of selenium and tellurium with sulfur- and selenium containing ligands, *Phosphorus Sulfur Relat. Elem.*, 1988, **38**, 271–280, DOI: **10.1080/03086648808079722**.
3 I. Haiduc, R. B. King and M. G. Newton, Stereochemical aspects of tellurium complexes with sulfur ligands: molecular compounds and supramolecular associations, *Chem. Rev.*, 1994, **94**, 301–326, DOI: **10.1021/cr00026a002**.
4 S. Husebye, Recent developments in the structural chemistry of tellurium with sulfur and selenium containing ligands, *Phosphorus, Sulfur Silicon Relat. Elem.*, 1998, **136**, 377–395, DOI: **10.1080/10426509808545965**.
5 I. Haiduc and J. Zukerman-Schpector, Supramolecular self-assembly through secondary bonds in organotellurium chemistry, *Phosphorus, Sulfur Silicon Relat. Elem.*, 2001, **171**, 171–185, DOI: **10.1080/10426500108046632**.
6 E. R. T. Tiekink and J. Zukerman-Schpector, Stereochemical activity of lone pairs of electrons and supramolecular aggregation patterns based on secondary interactions involving tellurium in its 1,1-dithiolate structures, *Coord. Chem. Rev.*, 2010, **254**, 46–76, DOI: **10.1016/j.ccr.2009.09.007**.
7 A. F. Cozzolino, P. J. W. Elder and I. Vargas-Baca, A survey of tellurium-centered secondary-bonding supramolecular synthons, *Coord. Chem. Rev.*, 2011, **255**, 1426–1438, DOI: **10.1016/j.ccr.2010.12.015**.
8 R. Gleiter, G. Haberhauer, D. B. Werz, F. Rominger and C. Bleiholder, From noncovalent chalcogen–chalcogen interactions to supramolecular aggregates: experiments and calculations, *Chem. Rev.*, 2018, **118**, 2010–2041, DOI: **10.1021/acs.chemrev.7b00449**.
9 E. R. T. Tiekink, Te···N secondary-bonding interactions in tellurium crystals: Supramolecular aggregation patterns and a comparison with their lighter congeners, *Coord. Chem. Rev.*, 2022, **457**, 214397, DOI: **10.1016/j.ccr.2021.214397**.
10 R. S. Mulliken, Structures of complexes formed by halogen molecules with aromatic and with oxygenated solvents, *J. Am. Chem. Soc.*, 1950, **72**, 600–608, DOI: **10.1021/ja01157a151**.
11 H. A. Bent, Structural chemistry of donor-acceptor interactions, *Chem. Rev.*, 1968, **68**, 587–648, DOI: **10.1021/cr60255a003**.

12 N. W. Alcock, Secondary bonding to nonmetallic elements, *Adv. Inorg. Chem. Radiochem.*, 1972, **15**, 1–58, DOI: **10.1016/S0065-2792(08)60016-3**.
13 J. Zukerman-Schpector and I. Haiduc, Tellurium···π-aryl interactions: a new bonding motif for supramolecular self-assembly and crystal engineering, *CrystEngComm*, 2002, **4**, 178–193, DOI: **10.1039/B201969H**.
14 E. R. T. Tiekink and J. Zukerman-Schpector, A structural survey of metal/π heteroaromatic supramolecular synthons for metal = tellurium, tin, and gold, *CrystEngComm*, 2009, **11**, 2701–2711, DOI: **10.1039/B910209D**.
15 I. Caracelli, J. Zukerman-Schpector, I. Haiduc and E. R. T. Tiekink, Main group metal lone-pair···π(arene) interactions: a new bonding mode for supramolecular associations, *CrystEngComm*, 2016, **18**, 6960–6978, DOI: **10.1039/C6CE01460G**.
16 T. Clark, M. Hennemann, J. S. Murray and P. Politzer, Halogen bonding: The σ-hole, *J. Mol. Model.*, 2007, **13**, 291–296, DOI: **10.1007/s00894-006-0130-2**.
17 J. S. Murray, P. Lane, T. Clark and P. Politzer, Sigma-hole bonding: molecules containing group VI atoms, *J. Mol. Model.*, 2007, **13**, 1033–1038, DOI: **10.1007/s00894-007-0225-4**.
18 P. Politzer and J. S. Murray, σ-Hole interactions: perspectives and misconceptions, *Crystals*, 2017, **7**, 212, DOI: **10.3390/cryst7070212**.
19 S. Scheiner, Competition between the two σ-holes in the formation of a chalcogen bond, *ChemPhysChem*, 2023, **24**, e202200936, DOI: **10.1002/cphc.202200936**.
20 H. Wang, J. Liu and W. Wang, *Phys. Chem. Chem. Phys.*, 2018, **20**, 5227–5234, DOI: **10.1039/C7CP08215K**.
21 A. Frontera and A. Bauzá, On the importance of σ-hole interactions in crystal structures, *Crystals*, 2021, **11**, 1205, DOI: **10.3390/cryst11101205**.
22 E. R. T. Tiekink, Zero-, one-, two- and three-dimensional supramolecular architectures sustained by Se ··O chalcogen bonding: A crystallographic survey, *Coord. Chem. Rev.*, 2021, **427**, 213586, DOI: **10.1016/j.ccr.2020.213586**.
23 E. R. T. Tiekink, Supramolecular aggregation patterns featuring Se···N secondary-bonding interactions in mononuclear selenium compounds: A comparison with their congeners, *Coord. Chem. Rev.*, 2021, **443**, 214031, DOI: **10.1016/j.ccr.2021.214031**.
24 E. R. T. Tiekink, Supramolecular architectures featuring Se···N secondary-bonding interactions in crystals of selenium-rich molecules: A comparison with their congeners, *CrystEngComm*, 2023, **25**, 9–39, DOI: **10.1039/d2ce01414a**.
25 I. Caracelli, J. Zukerman-Schpector and E. R. T. Tiekink, Supramolecular aggregation patterns based on the bio-inspired Se(lone pair)···π(aryl) synthon, *Coord. Chem. Rev.*, 2012, **256**, 412–438, DOI: **10.1016/j.ccr.2011.10.021**.
26 S. Burguera, R. M. Gomila, A. Bauzá and A. Frontera, Chalcogen bonds, halogen bonds and halogen···halogen contacts in di- and tri-iododiorganyltellurium(IV) derivatives, *Inorganics*, 2023, **11**, 209, DOI: **10.3390/inorganics11050209**.
27 J. S. Murray, P. Lane, T. Clark, K. E. Riley and P. Politzer, σ-Holes, π-holes and electrostatically-driven interactions, *J. Mol. Model.*, 2012, **18**, 541–548, DOI: **10.1007/s00894-011-1089-1**.
28 J. S. Murray and P. Politzer, Interaction and polarization energy relationships in σ-hole and π-hole bonding, *Crystals*, 2020, **10**, 76, DOI: **10.3390/cryst10020076**.
29 S. Scheiner, Dissection of the origin of π-holes and the noncovalent bonds in which they engage, *J. Phys. Chem. A*, 2021, **125**, 6514–6528, DOI: **10.1021/acs.jpca.1c05431**.
30 W. Zierkiewicz, M. Michalczyk and S. Scheiner, Noncovalent bonds through sigma and pi-hole located on the same molecule. guiding principles and comparisons, *Molecules*, 2021, **26**, 1740, DOI: **10.3390/molecules26061740**.
31 A. V. Rozhkov, M. V. Zhmykhova, Y. V. Torubaev, E. A. Katlenok, D. M. Kryukov and V. Yu. Kukushkin, Bis(perfluoroaryl)chalcolanes ArF_2Ch (Ch = S, Se, Te) as σ/π-hole donors for supramolecular applications based on noncovalent bonding, *Cryst. Growth Des.*, 2023, **23**, 2593–2601, DOI: **10.1021/acs.cgd.2c01454**.
32 B. Majhi, V. A. Lohar, P. Meena and D. Chopra, Quantitative investigation of intermolecular Te···A (A = π/Te/H) interactions in organotellurium compounds from the Cambridge Structural Database, *Cryst. Growth Des.*, 2023, **23**, 7922–7938, DOI: **10.1021/acs.cgd.3c00703**.
33 F. Lei, Q. Liu, Y. Zhong, X. Cui, J. Yu, Z. Hu, G. Feng, Z. Zeng and T. Lu, Computational insight into the nature and strength of the π-hole type chalcogen···chalcogen interactions in the $XO_2\cdots CH_3YCH_3$ complexes (X = S, Se, Te; Y = O, S, Se, Te), *Int. J. Mol. Sci.*, 2023, **24**, 16193, DOI: **10.3390/ijms242216193**.
34 E. A. Katlenok, M. L. Kuznetsov, N. A. Semenov, N. A. Bokach and V. Yu. Kukushkin, A new look at the chalcogen bond: π-hole-based chalcogen (Se, Te) bonding which does not include a σ-hole interaction, *Inorg. Chem. Front.*, 2023, **10**, 3065–3081, DOI: **10.1039/D3QI00087G**.
35 S. Bhandary, A. Sirohiwal, R. Kadu, S. Kumar and D. Chopra, Dispersion stabilized Se/Te···π double chalcogen bonding synthons in in situ cryocrystallized divalent organochalcogen liquids, *Cryst. Growth Des.*, 2018, **18**, 3734–3739, DOI: **10.1021/acs.cgd.8b00585**.
36 B. Zhou and F. P. Gabbaï, Anion chelation via double chalcogen bonding: the case of a bis-telluronium dication and its application in electrophilic catalysis via metal-chloride bond activation, *J. Am. Chem. Soc.*, 2021, **143**, 8625–8630, DOI: **10.1021/jacs.1c04482**.
37 C. Wölper, R. Gleiter and G. Haberhauer, Bifurcated chalcogen bonds based on one σ-hole, *Org. Mater.*, 2022, **4**, 43–52, DOI: **10.1055/a-1883-6076**.
38 Y. Wang, C. Zhao, W.-K. Chen and Y. Zeng, Chalcogen bond catalysis with telluronium cations for bromination reaction: importance of electrostatic and polarization effects, *Chem. – Eur. J.*, 2023, **29**, e202302749, DOI: **10.1002/chem.202302749**.
39 S. Ghinato, A. Giordana, E. Diana, R. M. Gomila, E. Priola and A. Frontera, Synthesis, X-ray characterization and DFT analysis of dicyanidoaurate telluronium salts: on the

importance of charge assisted chalcogen bonds, *Dalton Trans.*, 2023, **52**, 15688–15696, DOI: **10.1039/D3DT02787B**.

40 P. C. Ho, P. Szydlowski, J. Sinclair, P. J. W. Elder, J. Kübel, C. Gendy, L. M. Lee, H. Jenkins, J. F. Britten, D. R. Morim and I. Vargas-Baca, Supramolecular macrocycles reversibly assembled by Te···O chalcogen bonding, *Nat. Commun.*, 2016, **7**, 11299, DOI: **10.1038/ncomms11299**.

41 E. R. T. Tiekink, Supramolecular assembly based on "emerging" intermolecular interactions of particular interest to coordination chemists, *Coord. Chem. Rev.*, 2017, **345**, 209–228, DOI: **10.1016/j.ccr.2017.01.009**.

42 D. Dakternieks, R. Di Giacomo, R. W. Gable and B. F. Hoskins, Observation of secondary bonding in solution: synthesis, NMR studies, and the crystal structure of $Te^{VI}[OTe^{IV}(C_8H_8)(S_2P(OEt)_2)]_6$, *J. Am. Chem. Soc.*, 1988, **110**, 6541–6546, DOI: **10.1021/ja00227a040**.

43 P. J. W. Elder and I. Vargas-Baca, ^{125}Te NMR provides evidence of autoassociation of organo-ditellurides in solution, *Phys. Chem. Chem. Phys.*, 2016, **18**, 30740–30747, DOI: **10.1039/C6CP05892B**.

44 R. Weiss, E. Aubert, L. Groslambert, P. Pale and V. Mamane, Evidence for and evaluation of fluorine–tellurium chalcogen bonding, *Chem. Sci.*, 2023, **14**, 7221–7229, DOI: **10.1039/D3SC00849E**.

45 A. F. Cozzolino, G. Dimopoulos-Italiano, L. M. Lee and I. Vargas-Baca, *Eur. J. Inorg. Chem.*, 2013, **2013**, 2751–2756, DOI: **10.1002/ejic.201201439**.

46 L. Vogel, P. Wonner and S. M. Huber, Chalcogen bonding: An overview, *Angew. Chem., Int. Ed.*, 2019, **58**, 1880–1891, DOI: **10.1002/anie.201809432**.

47 A. Dhaka, I.-R. Jeon and M. Fourmigué, Selective activation of chalcogen bonding: an efficient structuring tool toward crystal engineering strategies, *Acc. Chem. Res.*, 2024, **57**, 362–374, DOI: **10.1021/acs.accounts.3c00674**.

48 K. T. Mahmudov, A. V. Gurbanov, V. A. Aliyeva, M. F. C. Guedes da Silva, G. Resnati and A. J. L. Pombeiro, Chalcogen bonding in coordination chemistry, *Coord. Chem. Rev.*, 2022, **464**, 214556, DOI: **10.1016/j.ccr.2022.214556**.

49 S. Benz, J. López-Andarias, J. Mareda, N. Sakai and S. Matile, Catalysis with chalcogen bonds, *Angew. Chem., Int. Ed.*, 2017, **56**, 812–815, DOI: **10.1002/anie.201611019**.

50 P. Pale and V. Mamane, Chalcogen bonding catalysis: tellurium, the last frontier?, *Chem. – Eur. J.*, 2023, **29**, e202302755, DOI: **10.1002/chem.202302755**.

51 N. Biot and D. Bonifazi, Chalcogen-bond driven molecular recognition at work, *Coord. Chem. Rev.*, 2020, **413**, 213243, DOI: **10.1016/j.ccr.2020.213243**.

52 K. T. Mahmudov, M. N. Kopylovich, M. F. C. Guedes da Silva and A. J. L. Pombeiro, Chalcogen bonding in synthesis, catalysis and design of materials, *Dalton Trans.*, 2017, **46**, 10121–10138, DOI: **10.1039/C7DT01685A**.

53 P. Scilabra, G. Terraneo and G. Resnati, The chalcogen bond in crystalline solids: a world parallel to halogen bond, *Acc. Chem. Res.*, 2019, **52**, 1313–1324, DOI: **10.1021/acs.accounts.9b00037**.

54 G. Cavallo, P. Metrangolo, R. Milani, T. Pilati, A. Priimagi, G. Resnati and G. Terraneo, The halogen bond, *Chem. Rev.*, 2016, **116**, 2478–2601, DOI: **10.1021/acs.chemrev.5b00484**.

55 S. Yamada and T. Tsutomu, Recent advances in halogen bond-assisted organic synthesis, *Curr. Org. Chem.*, 2020, **24**, 2118–2152, DOI: **10.2174/1385272823666191209112543**.

56 M. Breugst and J. J. Koenig, σ-Hole interactions in catalysis, *Eur. J. Org. Chem.*, 2020, **2020**, 5473–5487, DOI: **10.1002/ejoc.202000660**.

57 D. Devadiga and T. N. Ahipa, An up-to-date review on halogen-bonded liquid crystals, *J. Mol. Liq.*, 2021, **333**, 115961, DOI: **10.1016/j.molliq.2021.115961**.

58 H. Yang and M. W. Wong, Application of halogen bonding to organocatalysis: a theoretical perspective, *Molecules*, 2020, **25**, 1045, DOI: **10.3390/molecules25051045**.

59 R. Kampes, S. Zechel, M. D. Hager and U. S. Schubert, Halogen bonding in polymer science: towards new smart materials, *Chem. Sci.*, 2021, **12**, 9275–9286, DOI: **10.1039/D1SC02608A**.

60 W. Wang, Y. Zhang and W. J. Jin, Halogen bonding in room-temperature phosphorescent materials, *Coord. Chem. Rev.*, 2020, **404**, 213107, DOI: **10.1016/j.ccr.2019.213107**.

61 J. Pancholi and P. D. Beer, Halogen bonding motifs for anion recognition, *Coord. Chem. Rev.*, 2020, **416**, 213281, DOI: **10.1016/j.ccr.2020.213281**.

62 P. Metrangolo, H. Neukirch, T. Pilati and G. Resnati, Halogen bonding based recognition processes: a world parallel to hydrogen bonding, *Acc. Chem. Res.*, 2005, **38**, 386–395, DOI: **10.1021/ar0400995**.

63 A. Mukherjee, S. Tothadi and G. R. Desiraju, Halogen bonds in crystal engineering: Like hydrogen bonds yet different, *Acc. Chem. Res.*, 2014, **47**, 2514–2524, DOI: **10.1021/ar5001555**.

64 B. K. Saha, R. V. P. Veluthaparambath and V. G. Krishna, Halogen···halogen interactions: nature, directionality and applications, *Chem. – Asian J.*, 2023, **18**, e202300067, DOI: **10.1002/asia.202300067**.

65 E. R. T. Tiekink, Supramolecular architectures sustained by delocalised C–I···π(arene) interactions in molecular crystals and the propensity of their formation, *CrystEngComm*, 2021, **23**, 904–928, DOI: **10.1039/d0ce01677b**.

66 D. Schollmeyer, O. V. Shishkin, T. Rühl and M. O. Vysotsky, OH–π and halogen–π interactions as driving forces in the crystal organisations of tri-bromo and tri-iodo trityl alcohols, *CrystEngComm*, 2008, **10**, 715–723, DOI: **10.1039/B716442D**.

67 E. R. T. Tiekink, Characterising supramolecular architectures in crystals featuring I···Br halogen bonding: Persistence of X···X' secondary-bonding in their congeners, *Crystals*, 2021, **11**, 433, DOI: **10.3390/cryst11040433**.

68 T. Sakurai, M. Sundaralingam and G. A. Jeffrey, A nuclear quadrupole resonance and X-ray study of the crystal structure of 2,5-dichloroaniline, *Acta Crystallogr.*, 1963, **16**, 354–363, DOI: **10.1107/S0365110X63000979**.

69 G. R. Desiraju and R. Parthasarathy, The Nature of halogen···halogen interactions - are short halogen contacts due to specific attractive forces or due to close packing of

nonspherical atoms, *J. Am. Chem. Soc.*, 1989, **111**, 8725–8726, DOI: **10.1021/ja00205a027**.

70 A. J. Z. Londero, N. R. Pineda, V. Matos, P. C. Piquini, U. Abram and E. S. Lang, Synthesis and characterization of aryltellurium compounds including mixed-valence derivatives – evaluation of Te···S, Te···X and X···X (X = Br, I) interactions, *J. Organomet. Chem.*, 2020, **929**, 121553, DOI: **10.1016/j.jorganchem.2020.121553**.

71 Y. V. Torubaev, A. V. Rozhkov, I. V. Skabitsky, R. M. Gomila, A. Frontera and V. Yu. Kukushkin, Heterovalent chalcogen bonding: supramolecular assembly driven by the occurrence of a tellurium(II)···Ch(I) (Ch = S, Se, Te) linkage, *Inorg. Chem. Front.*, 2022, **9**, 5635–5644, DOI: **10.1039/D2QI01420C**.

72 C. R. Groom, I. J. Bruno, M. P. Lightfoot and S. C. Ward, The Cambridge Structural Database, *Acta Crystallogr., Sect. B: Struct. Sci., Cryst. Eng. Mater.*, 2016, **72**, 171–179, DOI: **10.1107/S2052520616003954**.

73 I. J. Bruno, J. C. Cole, P. R. Edgington, M. Kessler, C. F. Macrae, P. McCabe, J. Pearson and R. Taylor, New software for searching the Cambridge Structural Database and visualizing crystal structures, *Acta Crystallogr., Sect. B: Struct. Sci.*, 2002, **58**, 389–397, DOI: **10.1107/s0108768102003324**.

74 A. Bondi, van der Waals volumes and radii, *J. Phys. Chem.*, 1964, **68**, 441–451, DOI: **10.1021/j100785a001**.

75 A. Spek, checkCIF validation ALERTS: what they mean and how to respond, *Acta Crystallogr., Sect. E: Crystallogr. Commun.*, 2020, **76**, 1–11, DOI: **10.1107/S2056989019016244**.

76 K. Brandenburg, *DIAMOND*, Crystal Impact GbR, Bonn, Germany, 2006.

77 R. Ahlrichs, M. Bär, M. Häser, H. Horn and C. Kölmel, Electronic structure calculations on workstation computers: The program system Turbomole, *Chem. Phys. Lett.*, 1989, **162**, 165–169, DOI: **10.1016/0009-2614(89)85118-8**.

78 C. Adamo and V. Barone, Toward reliable density functional methods without adjustable parameters: The PBE0 model, *J. Chem. Phys.*, 1999, **110**, 6158–6170, DOI: **10.1063/1.478522**.

79 S. Grimme, J. Antony, S. Ehrlich and H. A. Krieg, Consistent and accurate *ab initio* parametrization of density functional dispersion correction (DFT-D) for the 94 elements H-Pu, *J. Chem. Phys.*, 2010, **132**, 154104, DOI: **10.1063/1.3382344**.

80 F. Weigend and R. Ahlrichs, Balanced basis sets of split valence, triple zeta valence and quadruple zeta valence quality for H to Rn: design and assessment of accuracy, *Phys. Chem. Chem. Phys.*, 2005, **7**, 3297–3305, DOI: **10.1039/b508541a**.

81 F. Weigend, Accurate coulomb-fitting basis sets for H to Rn, *Phys. Chem. Chem. Phys.*, 2006, **8**, 1057–1065, DOI: **10.1039/b515623h**.

82 K. Kupietz, R. M. Gomila, T. Roisnel, A. Frontera and R. Gramage-Doria, Shortening C≡N···Br–Csp^3 halogen bonds via π-stacking, *CrystEngComm*, 2024, **26**, 2131–2135, DOI: **10.1039/D4CE00307A**.

83 B. Mallada, A. Gallardo, M. Lamanec, B. de la Torre, V. Špirko, P. Hobza and P. Jelinek, Real-space imaging of anisotropic charge of σ-hole by means of Kelvin probe force microscopy, *Science*, 2021, **374**, 863–867, DOI: **10.1126/science.abk1479**.

84 R. F. W. Bader, A quantum theory of molecular structure and its applications, *Chem. Rev.*, 1991, **91**, 893–928, DOI: **10.1021/cr00005a013**.

85 W. Humphrey, A. Dalke and K. Schulten, VMD: Visual molecular dynamics, *J. Mol. Graphics*, 1996, **14**, 33–38, DOI: **10.1016/0263-7855(96)00018-5**.

86 E. D. Glendening, C. R. Landis and F. Weinhold, NBO 7.0: New vistas in localized and delocalized chemical bonding theory, *J. Comput. Chem.*, 2019, **40**, 2234–2241, DOI: **10.1002/JCC.25873**.

87 E. D. Glendening, J. K. Badenhoop, A. E. Reed, J. E. Carpenter, J. A. Bohmann, C. M. Morales, P. Karafiloglou, C. R. Landis and F. Weinhold, *NBO 7.0*, Theoretical Chemistry Institute, University of Wisconsin, Madison, WI, 2018.

88 G. M. de Oliveira, E. Faoro and E. S. Lang, New aryltellurenyl iodides with uncommon valences: Synthetic and structural characteristics of [$RTeTeI_2R$], [R_2TeTeR_2][Te_4I_{14}], and [RTe(I)I_2] (R = 2,6-dimethoxyphenyl), *Inorg. Chem.*, 2009, **48**, 4607–4609, DOI: **10.1021/ic900193k**.

89 Y. V. Torubaev, A. A. Pasynskii, A. V. Pavlova and M. M. Shaikh, Crystal structures of the products of unusual interactions between organotellurides and iodoacetylenes, *Mendeleev Commun.*, 2017, **27**, 141–143, DOI: **10.1016/j.mencom.2017.03.011**.

90 E. Faoro, G. M. de Oliveira and E. S. Lang, The intermediary RTeI as a source of new Te^{II} and Te^{IV} iodides by addition of (PyH)I and KI: synthesis and structural features of [{RTeI}{$RTeI_3$}]$_n$, [R_2Te–TeIR], (PyH)[$RTeI_2$] and (PyH)$_n$[RTeI(μ-I)TeIR]$_n$ (R = 2,6-dimethylphenyl; Py = pyridine), *J. Organomet. Chem.*, 2009, **694**, 1557–1561, DOI: **10.1016/j.jorganchem.2009.01.004**.

91 E. S. Lang, G. A. Casagrande, G. M. de Oliveira, G. N. Ledesma, S. S. Lemos, E. E. Castellano and U. Abram, One-pot synthesis and structure of organochalcogen halides with mixed valence states, *Eur. J. Inorg. Chem.*, 2006, **2006**, 958–964, DOI: **10.1002/ejic.200500803**.

92 Y. V. Torubaev, Chimeric supramolecular synthons in $Ph_2Te_2(I_2)Se$, *Acta Crystallogr., Sect. C: Struct. Chem.*, 2020, **76**, 579–584, DOI: **10.1107/S2053229620006166**.

93 N.-H. Hu, Z.-S. Jin and Z.-S. Li, Structure of hexamethylenetetratellurafulvalene diiodide, *Acta Crystallogr., Sect. C: Cryst. Struct. Commun.*, 1991, **47**, 1858–1860, DOI: **10.1107/S0108270191000495**.

94 V. Ganesh, M. Seshasayee, V. Kumar, S. Chidambaram, G. Aravamudan, K. Goubitz and H. Schenk, A novel mixed valence iodide bridged Te(II)-Te(IV) complex featuring diisopropyldithiocarbamate (L) and iodide: $ILTe^{II}(I)Te^{IV}L_2I$, *J. Crystallogr. Spectrosc. Res.*, 1989, **19**, 745–753, DOI: **10.1007/BF01179847**.